Inorg. Chem. **2006**, *45*, 8012–8025

Spectroscopic Methods in Bioinorganic Chemistry: Blue to Green to Red Copper Sites

Edward I. Solomon*

Department of Chemistry, Stanford University, Stanford, California 94305-5080

Received March 15, 2006

A wide variety of spectroscopic methods are now available that provide complimentary insights into the electronic structures of transition-metal complexes. Combined with calculations, these define key bonding interactions, enable the evaluation of reaction coordinates, and determine the origins of unique spectroscopic features/electronic structures that can activate metal centers for catalysis. This presentation will summarize the contributions of a range of spectroscopic methods combined with calculations in elucidating the electronic structure of an active site using the blue copper site as an example. The contribution of electronic structure to electron-transfer reactivity will be considered in terms of anisotropic covalency, electron-transfer pathways, reorganization energy, and protein contributions to the geometric and electronic structures of blue-copper-related active sites.

In bioinorganic chemistry, we focus on the small part of the large metalloprotein molecule that includes the metal ion and its local coordination environment (Figure 1).[1] This is the active site in catalysis and can be studied directly through the application of a wide variety of spectroscopic and magnetic methods.[2]

Figure 2 summarizes many of the key methods of physical−inorganic chemistry using the complete energy-level diagram of square-planar $CuCl_4^{2-}$ as a reference. The applications of many of these methods were discussed in detail in the symposium associated with this award.[3] Cu^{II} has nine valence d electrons resulting in one unpaired electron in the $d_{x^2-y^2}$ orbital in the ground state. This is perturbed by application of an external magnetic field and can be studied at low resolution by magnetic susceptibility to obtain the oxidation and spin state of the metal ion and at high resolution by magnetic Mössbauer (for ^{57}Fe) and electron paramagnetic resonance (EPR) based methods. These define the nature of the half-occupied orbital (i.e., $d_{x^2-y^2}$ vs d_{z^2}). The ground state can be studied at still higher resolution by double resonance (i.e., electron nuclear double resonance) and pulsed (i.e., electron spin−echo envelope modulation) EPR methods, which quantify the electron delocalization onto the ligands.

The above methods involve measurements in the energy region of $10^{-4}-10^{1}$ cm^{-1}. At higher photon energy (near-IR−vis, 4000−25 000 cm^{-1}), one excites electrons from filled d orbitals into the half-occupied d level. These d → d transitions are sensitive to the ligand field at the metal center and therefore provide a probe of the active-site geometric and electronic structures. These are parity-forbidden and

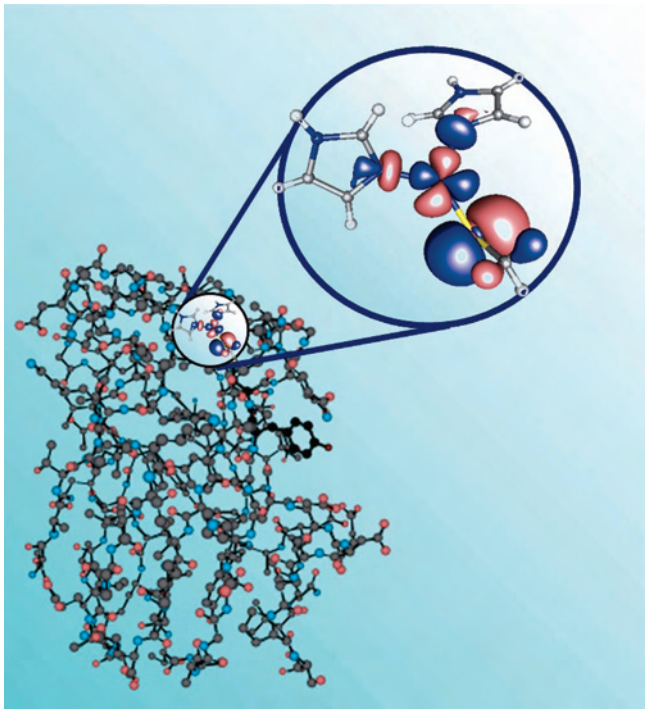

Figure 1. Crystal structure of plastocyanin (PDB code 1PLC) and an expanded view of the geometric and electronic structures of the active site.

* E-mail: edward.solomon@stanford.edu.

(1) Holm, R. H., Solomon, E. I., *Chem. Rev.* **1996**, *96* (thematic issue).
(2) Solomon, E. I., Lever, A. P. B., Eds. *Bioinorganic Spectroscopy*; Wiley: New York, 1999; Vols. I and II.
(3) *Abstracts of Papers*, 231st ACS National Meeting, Atlanta, GA, 2006; American Chemical Society: Washington, DC, 2006; INOR-316.

10.1021/ic060450d CCC: $33.50
Published on Web 08/12/2006

Edward I. Solomon grew up in North Miami Beach, FL, received his Ph.D. from Princeton University (with D. S. McClure), and was a postdoctoral fellow at the H. C. Orsted Institute (with C. J. Balhausen) and then at CalTech (with H. B. Gray). He was a professor at Massachusetts Institute of Technology until 1982. He then moved to Stanford University, where he is the Monroe E. Spaght Professor of Humanities and Sciences. He is a member of the National Academy of Sciences and the American Academy of Arts and Sciences and a Fellow of the American Association for the Advancement of Science. His awards include this American Chemical Society (ACS) award for Distinguished Service in the Advancement of Inorganic Chemistry, the ACS award in Inorganic Chemistry, the Remson Award from the Maryland ACS, the Centenary Medal of the Royal Society of Chemistry, the Wheland Medal from the University of Chicago, the Frontiers in Biological Chemisty Award from the Max Planck Institute in Mülheim, and the Deans Award for Distinguished Teaching at Stanford. He has presented a large number of named lectures including the first Glen Seaborg Lecture at the University of California—Berkeley and has been an Invited Professor at a number of international universities. His research is in the fields of physical—inorganic, theoretical—inorganic, and bioinorganic chemistry with emphasis on the application of a wide variety of spectroscopic and computational methods to elucidate the electronic structures of transition-metal complexes and their contributions to physical properties and reactivity. Areas of present interest are structure—function correlations in mono- and binuclear non-heme iron enzymes, O_2 and N_2O activation by mono-, bi-, tri-, and tetranuclear copper active sites, and electronic structure contributions to electron transfer in copper, iron—sulfur, and heme sites.

therefore weak in the absorption spectrum, but they can be intense in circular dichroism (CD) and magnetic CD (MCD) spectroscopies based on the different selection rules associated with each of these methods (to be discussed in a later section for low-temperature MCD).

At still higher energy (UV—vis), electrons are excited from the filled ligand-centered orbitals to the half-occupied d orbital, producing ligand-to-metal charge-transfer transitions. These involve a change in the electron density and therefore can be intense in the absorption spectrum. They are also polarized along the ligand—metal bond involved, allowing spectral assignment based on polarized single-crystal spectroscopy. Methods have also been developed [i.e., variable-temperature, variable-field MCD and optically detected magnetic resonance] to obtain polarized single-crystal-like data from a frozen solution.[4,5] The charge-transfer transitions are key to understanding the nature of ligand—metal bonds because high covalency is associated with low-energy, intense charge-transfer transitions.[6] The high intensity of these transitions further allows resonance enhancement of a Raman spectrum, which provides a probe of both active-site vibrations and the nature of the excited-state distortion.

To still higher energy, electrons are excited from core levels. The most familiar of those methods is extended X-ray absorption fine structure (EXAFS) in X-ray absorption spectroscopy (XAS), where the metal 1s electrons are excited into the continuum, scatter off adjacent atoms, and produce constructive and destructive interference with the outgoing electron wave, which gives geometric structural information on the active site. However, in XAS, one also observes transitions to bound states. For copper, the K edge is at ~8980 eV and the L edge is at ~930 eV, and for the chloride ligands in this reference complex, the K edge is at 2820 eV. It will be shown later in this presentation that spectra taken at these edges provide a direct experimental probe of the mixing and delocalization of the ground-state wave function over the active site.

The above spectroscopic methods experimentally measure the electronic structure of a transition-metal complex. It is important to correlate experiment with theory, and for transition-metal complexes, these are divided into two classes of calculations. Ligand-field theory focuses on the ground state and ligand-field excited states and describes their interaction with the coordination environment.[7] Ligand-field theory works very well as long as the metal site is not very covalent. When it is, one turns to molecular orbital theory, and for the large complexes of interest in bioinorganic chemistry, modern molecular orbital theory employs density functional theory (DFT).[8] Here it is important to emphasize that there are many functionals, hybrids, and other parameters in these calculations, which give different results. Thus, it is of critical importance to correlate modern DFT calculations with experiment.[9] Then calculations supported by data can be used to obtain further insight into electronic structure and its contribution to reactivity.

The goals of spectroscopy in bioinorganic chemistry are to determine active-site geometric and electronic structures and to develop structure—function correlations. Spectroscopy probes reaction mechanisms on a molecular level and defines key contributions to catalysis. This often involves using rapid freeze quench methods to trap intermediates, which can then be studied in detail using the above spectroscopic methods. To achieve these goals, one often has to develop new spectroscopic methods (where existing probes are not available or give ambiguous results) or to understand unique spectroscopic features (compared to small-molecule complexes of the same metal ion). We have shown that these unique spectroscopic features (i.e., low-energy, intense absorption features and unusual ground-state spin Hamiltonian parameters) reflect highly covalent active sites that can activate the metal center for catalysis.[6]

This presentation will illustrate many of the above concepts using the blue copper protein active site as an example.

(4) Neese, F.; Solomon, E. I. *Inorg. Chem.* **1999**, *38*, 1847—1865.
(5) Börger, B.; Bingham, S. J.; Gutschank, J.; Schweika, M. O.; Suter, D.; Thomson, A. J. *J. Chem. Phys.* **1999**, *111*, 8565—8568.
(6) Solomon, E. I.; Lowery, M. D. *Science* **1993**, 1575.
(7) Ballhausen, C. J. *Introduction to Ligand Field Theory*; McGraw-Hill: New York, 1962.
(8) Kohn, W.; Sham, L. J. *Phys. Rev.* **1965**, *140*, A1133.
(9) Szilagyi, R. K.; Metz, M.; Solomon, E. I. *J. Phys. Chem.* **2002**, *106*, 2994.

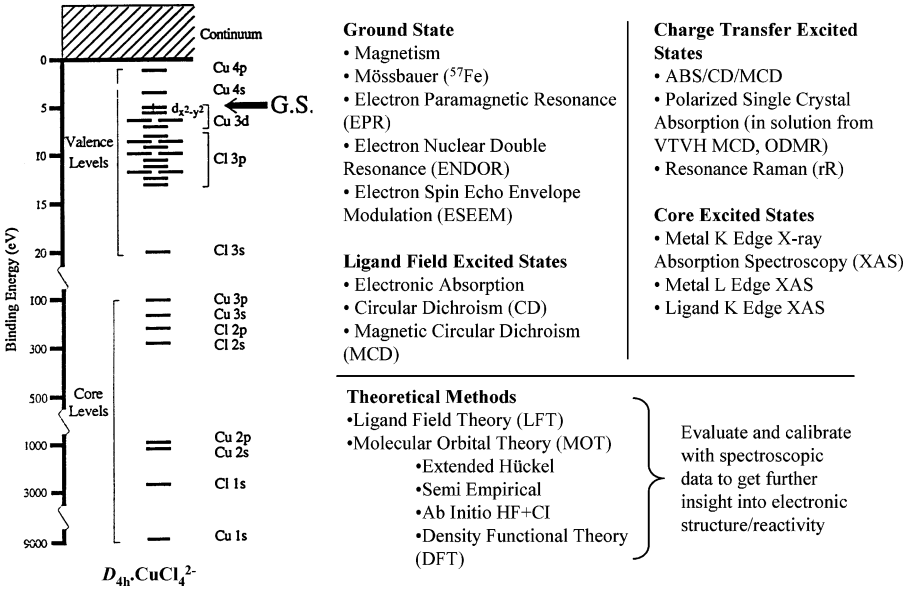

Figure 2. Complete molecular orbital energy-level diagram of $[CuCl_4]^{2-}$ (left) and an overview of different spectroscopic and theoretical methods to probe the ground and excited states (right).

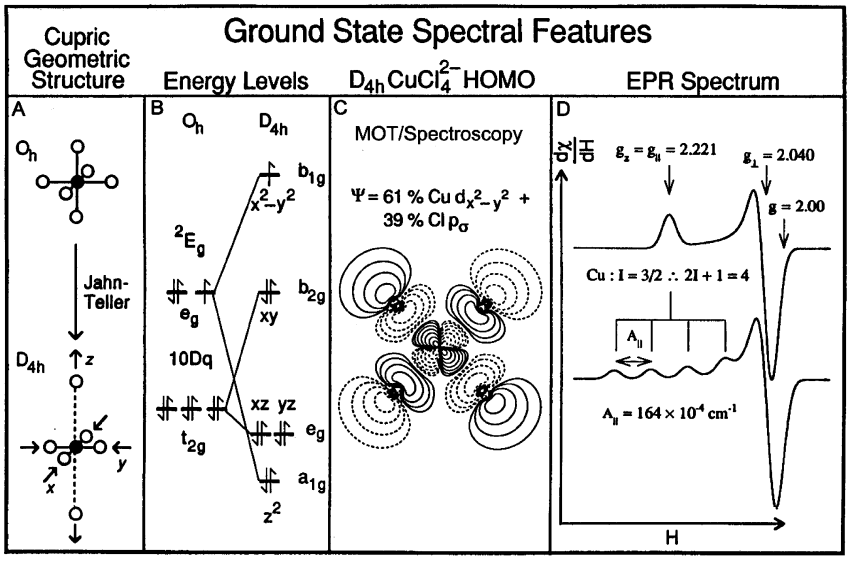

Figure 3. Ground-state spectral features of D_{4h} $[CuCl_4]^{2-}$: [(A) top and (B) left] O_h ligand field giving a d^9 ^2E_g ground state; [(A) bottom and (B) right] tetragonal Jahn−Teller distortion producing a $d_{x^2-y^2}$ ground state; (C) molecular orbital description of the "$d_{x^2-y^2}$" ground state of D_{4h} $CuCl_4^{2-}$; (D) EPR spectroscopy of tetragonal Cu^{II} complexes (top) without and (bottom) with hyperfine coupling to the copper nucleus ($I = {}^3/_2$).

However, because this presentation will focus on the origin of unique spectroscopic features, it is important to first consider the "normal" spectroscopy of cupric complexes using square-planar $CuCl_4^{2-}$ as a reference.[10]

Normal Copper Complexes. When a cupric ion is placed in an octahedral ligand field, the five d orbitals split into t_{2g} and e_g sets, separated in energy by the historical parameter of ligand-field theory 10*Dq* (*D* relating to the ligand electrostatic charge distribution and *q* the radial integral over the electron coordinates). Placing nine electrons into these ligand-field split orbitals gives one hole in the e_g set and thus a ^2E_g ground state. This is orbitally degenerate and thus unstable to a Jahn−Teller distortion of the molecule, which splits the degeneracy and lowers the energy of the complex. The generally observed Jahn−Teller distortion for cupric complexes is a tetragonal elongation along *z* and contraction in the equatorial plane leading to the square-planar $CuCl_4^{2-}$ limiting structure (Figure 3A). A key feature of ligand-field theory is that the splitting of the d orbitals is very dependent on the ligand environment around the metal center and is different for square planar relative to octahedral coordination. The d orbital splitting appropriate for D_{4h} $CuCl_4^{2-}$ is given in Figure 3B, with the highest-energy half-occupied d orbital being $d_{x^2-y^2}$ because its lobes point directly at the ligands and thus it has the largest repulsive or antibonding interaction with the ligand field. These, however, are not pure d orbitals but are involved in bonding/antibonding interactions with the ligands that are given by molecular orbital theory. The most accurate DFT calculated/experimentally supported description of the ground state of square-planar cupric chloride is given in Figure 3C; it has 61% Cu $d_{x^2-y^2}$ character, with the rest of the wave function equivalently delocalized

(10) Solomon, E. I. In *Comments on Inorganic Chemistry*; Sutin, N., Ed.; Gordon and Breach: New York, 1984; Vol. III, p 225.

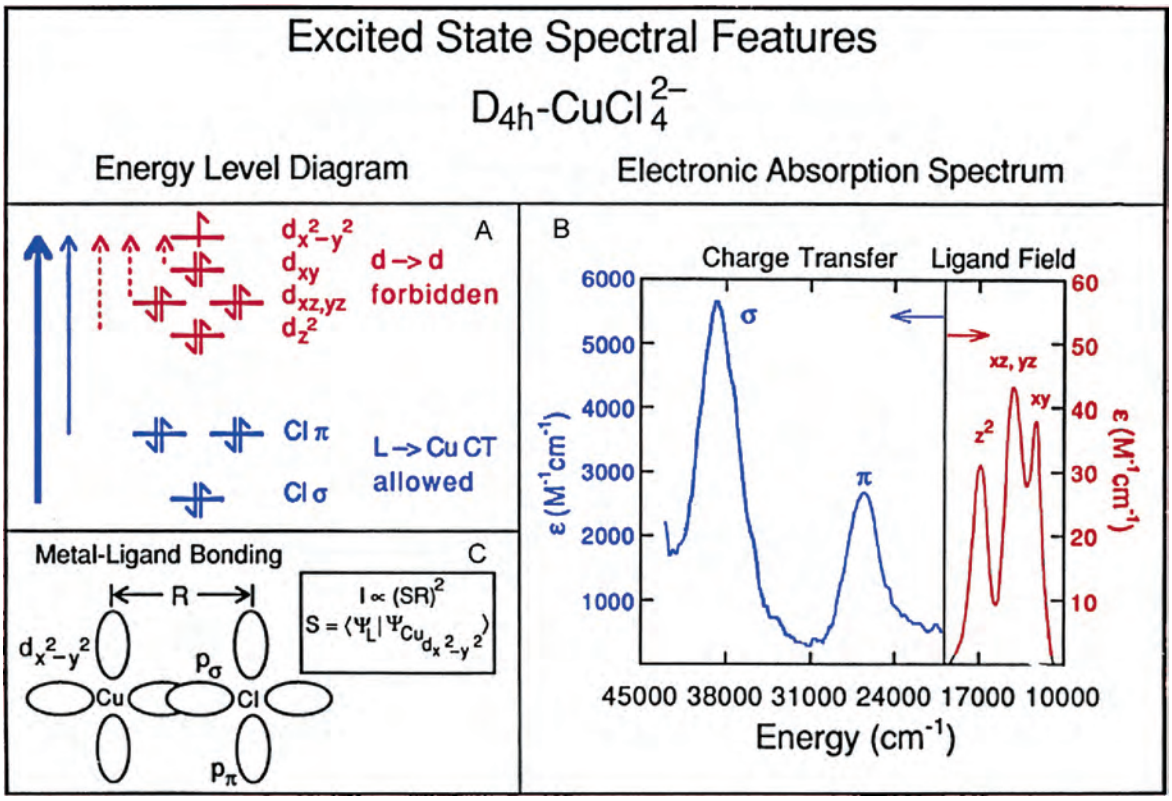

Figure 4. Excited-state spectral features of D_{4h} $[CuCl_4]^{2-}$: (A) ligand-field and ligand-to-metal charge-transfer transitions (arrow width gives intensity); (B) ligand-field (red) and charge-transfer (blue) transitions of D_{4h} $CuCl_4^{2}$; (C) three valence 3p orbitals on chloride split due to σ/π bonding to copper. The charge-transfer intensity is given by overlap of the donor and acceptor orbitals.

over the four chloride ligands (as required by group theory), which are involved in σ-antibonding interactions with the copper.

The ground state of D_{4h} $CuCl_4^{2-}$ thus has one unpaired electron in this $d_{x^2-y^2}$-derived molecular orbital and is studied by EPR spectroscopy. It exhibits a spectrum with $g_{\|} > g_{\perp} > 2.0023$, which from ligand-field theory is characteristic of a $d_{x^2-y^2}$ ground state. It should be noted that the spectrum shown at the top of Figure 3D would be that of a frozen solution with all orientations of the copper site. This spectrum is plotted as the first derivative, which is measured to increase sensitivity, leading to a peak at $g_{\|}$ and a more intense derivative-shaped feature at $g_{\perp}$. This is a theoretical spectrum because copper has a nucleus spin of $I = {}^3/_2$, which will couple to the electron spin to produce a hyperfine splitting into $2I + 1 = 4$ lines. The hyperfine splitting in the $g_{\|}$ region, $A_{\|}$, is large, $\sim|164| \times 10^{-4}$ cm^{-1} for D_{4h} $CuCl_4^{2-}$, while $A_{\perp}$ is much smaller and not resolvable in the $g_{\perp}$ region.

Going up in energy (near-IR−vis), electrons are excited from filled d orbitals into the half-occupied $d_{x^2-y^2}$ level, leading to the ligand-field transitions. As indicated in Figure 4A red, these are parity-forbidden (i.e., Laporté) and hence weak in the absorption spectrum in the low-energy region ($\sim$16 000 cm^{-1}; $\epsilon \sim 40$ M^{-1} cm^{-1}; Figure 4B red). At higher energy (Figure 4A blue), electrons from filled ligand-based molecular orbitals are excited into the half-occupied $d_{x^2-y^2}$ orbital, leading to the ligand-to-metal charge-transfer transitions. From Figure 4B blue, these are intense transitions at higher energy (25 000−40 000 cm^{-1}; $\epsilon \sim$ 2000−5000 M^{-1} cm^{-1}) relative to the ligand-field transitions. They provide detailed insight into the nature of the ligand−metal bonds. Chloride has three valence 3p orbitals, which split into two sets upon binding to copper (Figure 4A blue): pσ at deeper energy because it is σ-bonding to the metal (i.e., oriented along the ligand−metal bond) and the pπ set (in and out of plane, perpendicular to the ligand−metal bond) at lower energy. The intensities of these transitions are proportional to the overlap of the donor and acceptor orbitals involved in the charge-transfer process. From Figure 4C, excitation from pσ will produce an intense charge-transfer transition (due to its σ overlap with $d_{x^2-y^2}$) while charge transfer from the chloride pπ will be weak because the intensity is only derived from configuration interaction (i.e., mixing with intense charge-transfer transitions of the same symmetry).[11] Thus, for normal ligand−metal bonding, a lobe of the $d_{x^2-y^2}$ orbital is oriented along the ligand−metal bond and there is σ overlap. This results in a low-energy, weak π and high-energy, intense σ charge-transfer pattern, which is also experimentally observed (Figure 4B blue) and is characteristic of a normal ligand−metal bond.

Electron-Transfer (ET) Sites in Bioinorganic Chemistry. Figure 5 summarizes most of the key metal centers involved in biological ET.[12] For copper, these are the blue copper site, the focus of this presentation, and the mixed-valent binuclear Cu_A center. For Cu_A, the coppers are bridged by thiolates and there is also a weak direct Cu−Cu bond, which maintains electron delocalization even in the low-symmetry protein environment.[13] For iron, the ET sites include the 1, 2, 3, and 4 iron−sulfur centers, which have high-spin tetrahedral metal sites, and the cytochromes, which

(11) Desjardins, S. R.; Penfield, K. W.; Cohen, S. L.; Musselman, R. L.; Solomon, E. I. *J. Am. Chem. Soc.* **1983**, *105*, 4590.
(12) Holm, R. H.; Kennepohl, P.; Solomon, E. I. *Chem. Rev.* **1996**, *96*, 2239.

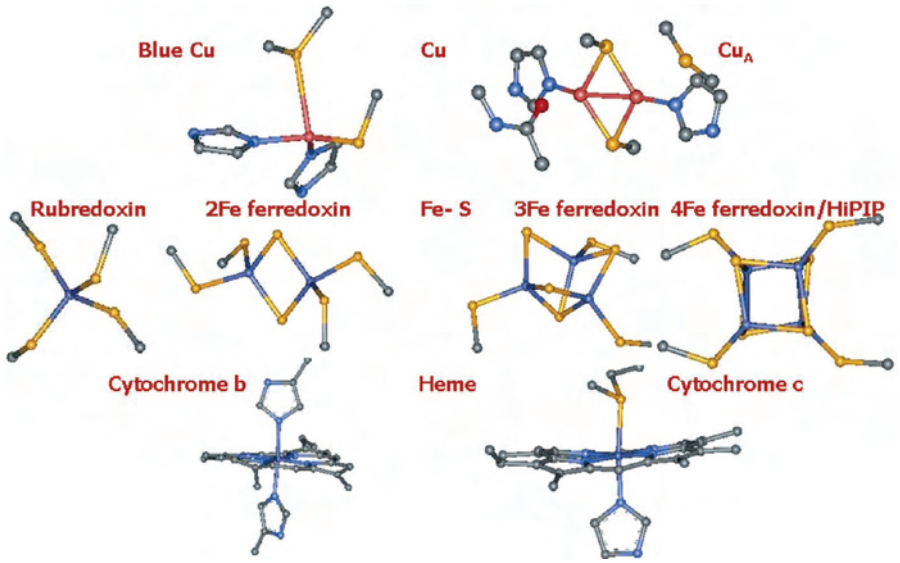

Figure 5. ET sites in bioinorganic chemistry.

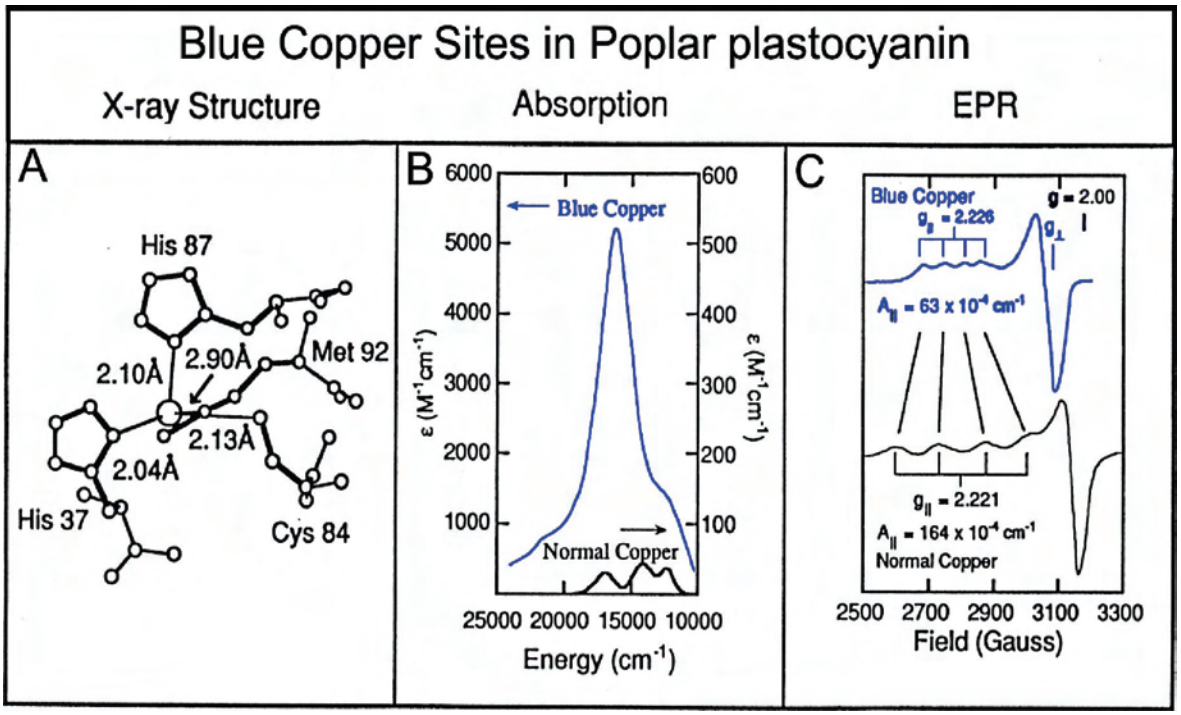

Figure 6. (A) X-ray structure of the blue copper site in poplar plastocyanin.[16] (B) Absorption spectrum of plastocyanin (left ϵ scale) and "normal" D_{4h} $[CuCl_4]^{2-}$ (right ϵ scale). (C) X-band EPR spectrum of plastocyanin (top) and D_{4h} $[CuCl_4]^{2-}$ (bottom).

have low-spin six-coordinate heme sites. In all cases for efficient ET, there is minimal change in geometry with redox (i.e., a low reorganizational energy λ in Marcus theory[14]) and efficient electronic coupling through the protein [i.e., a large $\mathbf{H}_{DA}$ matrix element for coupling the donor (D) and acceptor (A)]. Here we focus on the blue-copper-related sites, their unique spectroscopic features and how these reflect a novel electronic structure that results in a low λ and a large $\mathbf{H}_{DA}$, and the role of the protein in determining the geometric and electronic structures of blue-copper-related sites.[15]

Unique Spectroscopic Features of Oxidized Blue Copper Sites. This overview starts in 1978 when Hans Freeman determined the crystal structure of the first blue copper site, that of plastocyanin, which couples photosystem I with photosystem II through ET.[16] The geometric structure of the copper site was distorted tetrahedral, not the tetragonal structure normally observed for cupric complexes (Figure 6A), which raised the issue of the role of protein in determining the geometric structure of this active site. There were also two chemically interesting ligands: a short thiolate sulfur of Cys with a Cu−S bond length of ~2.1 Å and a

(13) Gamelin, D. R.; Randall, D. W.; Hay, M. T.; Houser, R. P.; Mulder, T. C.; Canters, G. W.; de Vries, S.; Tolman, W. B.; Lu, Y.; Solomon, E. I. *J. Am. Chem. Soc.* **1998**, *120*, 5246.
(14) Marcus, R. A.; Sutin, N. *Biochim. Biophys. Acta* **1985**, *811*, 265−322.
(15) Solomon, E. I.; Szilagyi, R. K.; George, S. D.; Basumallick, L. *Chem. Rev.* **2004**, *104*, 419.
(16) Colman, P. M.; Freeman, H. C.; Guss, J. M.; Murata, M.; Norris, V. A.; Ramshaw, J. A. M.; Venkatappa, M. P. *Nature* **1978**, *272*, 319.

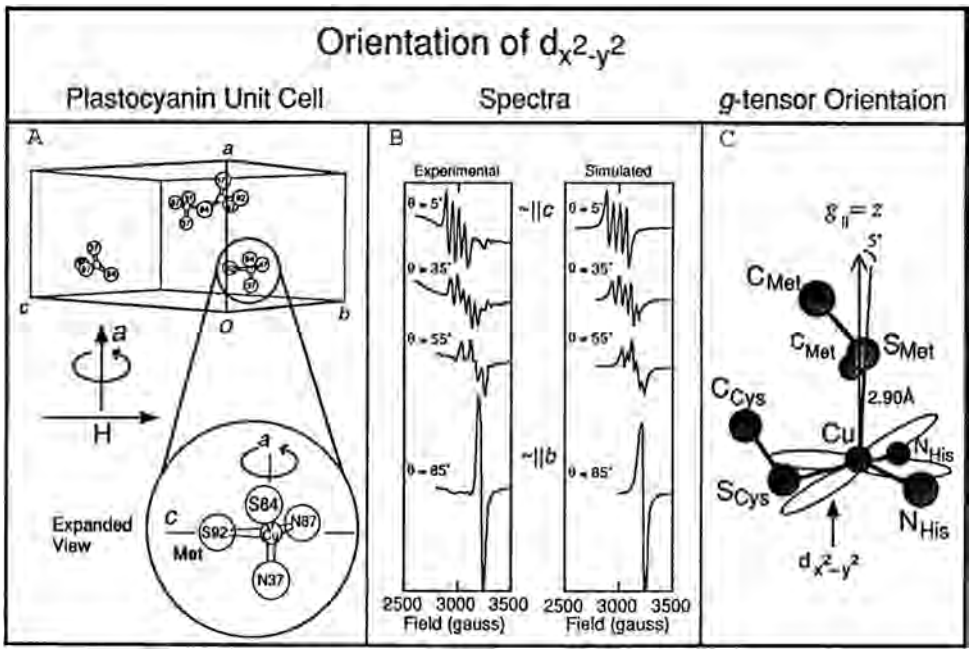

Figure 7. Single-crystal EPR of poplar plastocyanin; orientation of the $d_{x^2-y^2}$ orbital. (A) Unit cell and molecular orientation of poplar plastocyanin with respect to the applied magnetic field. θ is the angle between the magnetic field (**H**) and the crystallographic *c* axis ($\theta = 0$; **H** and *c* are collinear). (B) EPR spectra (left) and simulations (right) for the crystal orientations shown. (C) Orientation of the $g_{||}$ direction and the $d_{x^2-y^2}$ orbital superimposed on the blue copper site.

long thioether S−Cu bond of Met at a distance of ∼2.9 Å from the copper. The coordination environment was completed by two fairly normal His N−Cu bonds at ∼2.05 Å.

Associated with this unusual geometry and ligation are the unique spectroscopic features of the blue copper site. In contrast to the weak d → d transitions of normal tetragonal Cu^{II} complexes with $\epsilon \sim 40\ M^{-1}\ cm^{-1}$ at ∼16 000 cm^{-1}, the blue copper site has an intense absorption band at 16 000 cm^{-1} (∼600 nm) with $\epsilon \sim 5000\ M^{-1}\ cm^{-1}$ (Figure 6B). In the ground-state EPR spectrum (Figure 6C), the hyperfine coupling ($A_{||}$) of the electron spin to the nuclear spin on the copper is reduced by more than a factor of 2 for blue copper relative to normal copper complexes. We now consider the origin of these unique spectroscopic features. These reflect a novel ground-state wave function that is extremely important to understand because it is the redox-active molecular orbital (RAMO) that plays the key role in biological function, long-range rapid ET to a specific position in the protein.

Nature of the Ground-State Wave Function. From Figure 6C, the blue copper site has $g_{||} > g_{\perp} > 2.0023$ and therefore a $d_{x^2-y^2}$ ground state. The first goal of spectroscopy was to determine the orientation of this orbital in the distorted tetrahedral ligand field of the blue copper site (Figure 6A). This was accomplished through single-crystal EPR spectroscopy.[17] Plastocyanin crystallizes in an orthorhombic space group with four molecules in the unit cell. Their active sites are shown on an expanded scale in Figure 7A. Here, the EPR data are given for the field in the *bc* plane and the crystal is rotated around the *a* axis. From Figure 7B left, a $g_{||}$ spectrum (with the four $A_{||}$ hyperfine lines) is observed with the field along the *c* axis, while a $g_{\perp}$ spectrum is obtained when the field is rotated 90° off the *c* axis. Thus, the $g_{||}$ direction is approximately along the *c* axis, which from Figure 7A is approximately along the long Met S−Cu bond. A series of experimental single-crystal rotations were performed, and the data were simulated with four molecules in the unit cell. This gave the specific orientation of $g_{||}$ shown in Figure 7C, which is tilted just 5° off the long thioether S−Cu bond. This defines the electronic *z* axis and puts the $d_{x^2-y^2}$ orbital (perpendicular to *z*) within 15° of the plane defined by the three strong ligands: the Cys S and two His N ligands. From this point in the presentation, the ground state will be pictured in this *xy* plane.

The second feature of the ground state to be considered is the origin of the small $A_{||}$ value of the blue copper site. From Figure 8, there are three contributions to the hyperfine coupling of the unpaired electron to the nuclear spin of the copper. The Fermi contact term involves interaction with the electron spin density at the nucleus. Because an unpaired electron in the $d_{x^2-y^2}$ orbital has no probability at the nucleus, this results from spin polarization of core s electrons, mostly 2s, such that the α and β electrons have different probabilities at the nucleus, producing a net large negative contribution to the hyperfine coupling. The spin dipolar term is classical and involves the dipolar coupling of the electron spin position averaged over the $d_{x^2-y^2}$ orbital with the nuclear spin on the copper. This is also large and negative. The orbital dipolar term has an origin similar to that of the *g* values deviating from 2.0023, which will be considered later, and can be calculated from the experimental *g* values. For square-planar $CuCl_4^{2-}$, these three terms are of similar large magnitude and the orbital dipolar term is of positive sign, leading to the net large magnitude of the $A_{||}$ value observed experimentally. For blue copper, $A_{||}$ is greatly decreased in magnitude, and the initial explanation for this focused on the spin dipolar term and the distorted tetrahedral geometry of the blue copper site. It was thought that the distorted tetrahedral structure would allow the Cu $4p_z$ orbital to mix with the Cu $d_{x^2-y^2}$ orbital. An electron averaged over the p_z orbital would have the opposite sign for its spin dipolar

(17) Penfield, K. W.; Gay, R. R.; Himmelwright, R. S.; Eickman, N. C.; Norris, V. A.; Freeman, H. C.; Solomon, E. I. *J. Am. Chem. Soc.* **1981**, *103*, 4382.

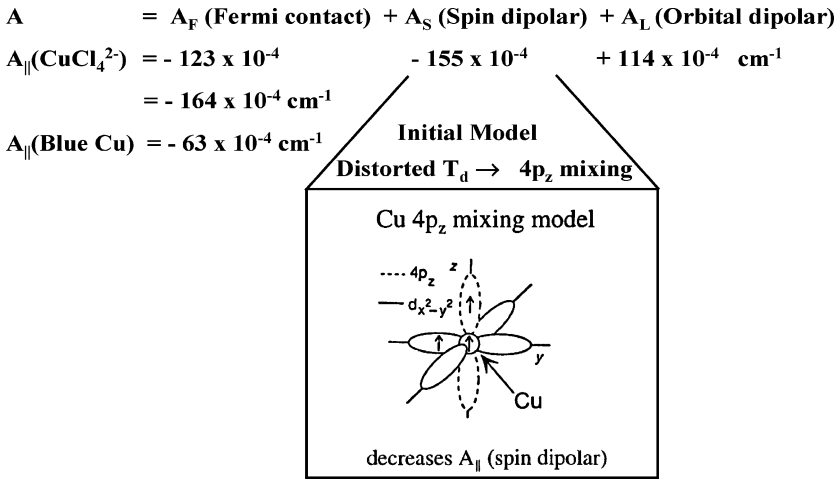

Figure 8. Geometric distortion model for small $A_{||}$ values. Cu $4p_z$ mixes with the $d_{x^2-y^2}$ orbital in D_{2d} symmetry.

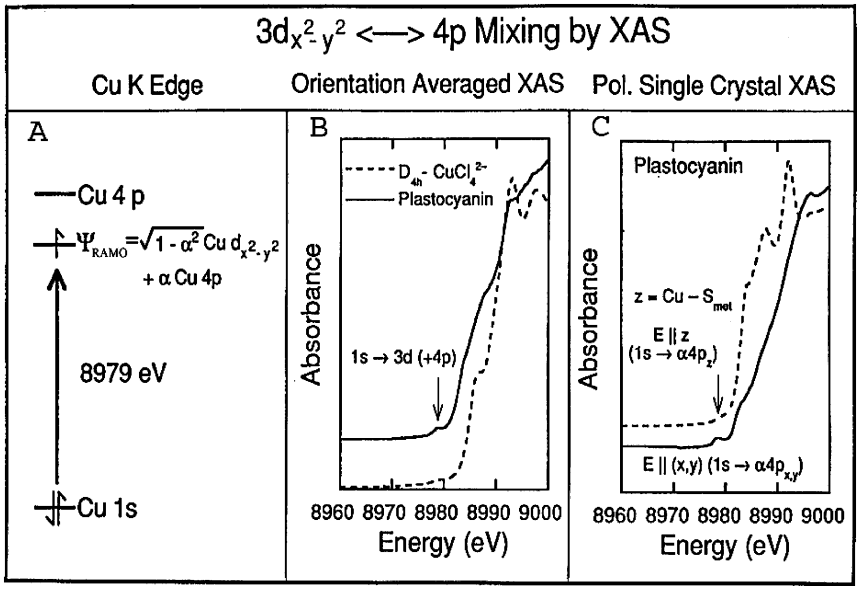

Figure 9. Cu K-edge XAS: (A) energy-level diagram giving Cu 1s to RAMO transition; (B) orientation-averaged XAS spectra of D_{4h} $[CuCl_4]^{2-}$ and the blue copper site in poplar plastocyanin; (C) polarized single-crystal XAS spectra[19] for the poplar plastocyanin.

interaction, and if there were 12% Cu $4p_z$ mixing, this would reduce the $A_{||}$ value to that of the blue copper site.

Thus, one had to experimentally determine the Cu 4p mixing into the $d_{x^2-y^2}$ orbital. This was accomplished by going up 10 orders of magnitude in photon energy (from the 10^{-4}-cm^{-1} region of hyperfine coupling) to ~9000 eV, the Cu K edge in XAS.[18] From Figure 9A, at 8979 eV there is a transition from the Cu 1s orbital to the half-occupied RAMO. Because s → d is electric-dipole-forbidden, the dominant intensity in this preedge transition would derive from any Cu 4p mixing due to the distorted tetrahedral environment because s → p is electric-dipole-allowed. From Figure 9B, square-planar $CuCl_4^{2-}$ has very little intensity in the preedge (arrow at 8979 eV) consistent with its center of inversion; hence, d/p mixing is forbidden. In going to plastocyanin, the intensity of the 8979-eV transition increases, reflecting 4p mixing into the $d_{x^2-y^2}$ orbital in the distorted tetrahedral environment of blue copper. The nature of this mixing could be determined from polarized edge data. In Figure 9C, the dashed spectrum[19] reflects the edge taken with the **E** vector of light oriented along the *z* axis, which was determined from the single-crystal EPR data presented earlier. This is the orientation where the intensity associated with $4p_z$ mixing would be observed, and there is none. The solid XAS spectrum is for light polarized in the *xy* plane. All of the preedge intensity is present in this polarization, indicating that the $d_{x^2-y^2}$ orbital mixes with the Cu $4p_{x,y}$ orbital. This would have the same sign for the spin dipolar term and could not decrease the hyperfine coupling.

The above XAS experiment at the Cu K edge eliminated the generally accepted explanation for the small $A_{||}$ value of blue copper. We thus focused on the alternative possible explanation for the small hyperfine coupling, a highly covalent site. Covalency delocalizes the electron spin off the copper center and would reduce its hyperfine coupling with the nuclear spin on the copper. Hence, we turned to molecular orbital theory and a quantitative consideration of the EPR *g* values of the blue copper site.[20]

(18) Shadle, S. E.; Penner-Hahn, J. E.; Schugar, H.; Hedman, B.; Hodgson, K. O.; Solomon, E. I. *J. Am. Chem. Soc.* **1993**, *115*, 767.

(19) Scott, R. A.; Hahn, J. E.; Doniach, S.; Freeman, H. C.; Hodgson, K. O. *J. Am. Chem. Soc.* **1982**, *104*, 5364.

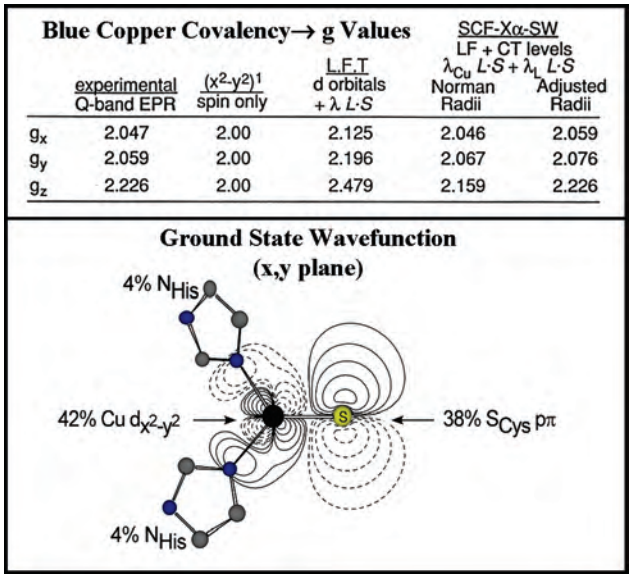

Figure 10. Quantitative analysis of *g* values for plastocyanin (top). Contour of plastocyanin ground-state wave function (RAMO) calculated by SCF-Xα-SW adjusted to spectroscopic data (bottom).

From Figure 10 top, the blue copper site in plastocyanin has $g_{\|} > g_{\perp} > 2.0023$, indicating an unpaired electron in a $d_{x^2-y^2}$ orbital. However, if this limiting description were appropriate, there would only be spin angular momentum and the *g* values would be 2.0023 and isotropic. Ligand-field theory allows for spin−orbit coupling of the ground state with ligand-field excited states. This mixes orbital angular momentum into the ground state and leads to *g* values that deviate from 2.0023. From the third column in the table at the top of Figure 10, a complete ligand-field calculation of the blue copper sites gives $g_{\|} > g_{\perp} > 2.0023$, consistent with a $d_{x^2-y^2}$ ground state; however, the calculated *g* values deviate too much from 2.0023 relative to experiment (first column in the table). This indicated that there was too much orbital angular momentum in the ligand-field calculation. This treats the d orbitals as localized on the copper while delocalization onto the ligands reduces the orbital angular momentum and thus the calculated *g* values. We then turned to molecular orbital theory, and in the early days of DFT (i.e., early 1980s), this was the SCF-xα-SW (self-consistent-field xα-scattered wave) approach.[21] A calculation performed with the standard methodology at the time (i.e., the Norman radii column[22]) did reduce the calculated *g* values relative to those calculated by ligand-field theory. However, compared to experiment (first column), these were too close to 2.0023, indicating that the standard SCF-xα-SW calculation was giving too covalent a description of the ground state. The last step was to adjust the parameters of the calculation (the scattered wave radii) until the calculation reproduced the experimental *g* values and thus gave an experimentally adjusted description of the ground state of the blue copper site.[20] This is shown at the bottom of Figure 10 in the *xy* plane defined by Cu, Cys S, and two His N. This site is highly covalent with 42% Cu $d_{x^2-y^2}$ character, and the covalency is highly anisotropic, with delocalization dominantly into the pπ orbital of the Cys S.

Modern DFT. The ground-state description in Figure 10 was developed in 1985. The DFT methodology has advanced greatly since that time, allowing total energy calculations, geometry optimizations, and evaluation of reaction coordinates.[23,24] All modern DFT calculations give qualitatively the same description of the ground state of the blue copper site, a highly covalent site with the covalency delocalized into the pπ orbital of the thiolate sulfur (Figure 11 left).[15,25,26] However, standard modern DFT calculations, in fact, give sites that are overly covalent relative to experiment with ∼30% Cu and ∼60% Cys S character (experimental values are given in green in the table in Figure 11 with 41% Cu d and 38% S p character). BP86 is a pure functional, while the B3LYP calculation is a hybrid with ∼20% Hartree−Fock exchange mixing. For a small cluster model of the blue copper site with 33 atoms, our approach has been to adjust the calculations to better correlate with experiment by increasing the Hartree−Fock mixing in the hybrid, which decreases the covalency, as does decreasing Z_{eff} on the copper (as in the ADF package).[9,15,26]

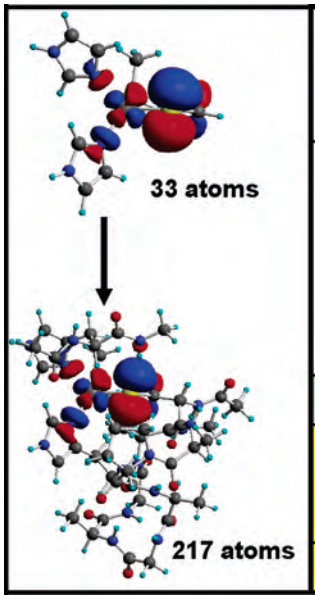

Model	Functional	Atomic Spin Density	
		Cu	S_{Cys}
33-atom QM	BP86	0.27	0.61
	B3LYP	0.33	0.57
	BP86, adjusted Z_{eff}	0.49	0.42
	B(38HF)P86	0.46	0.44
Experiment (XAS)		0.41 d	0.38 p
217-atom QM (includes protein dipoles and H-bond to S_{Cys})	B3LYP	0.43	0.43
QM/MM, all protein	B3LYP	0.44	0.42

Figure 11. Blue copper ground-state wave function by modern DFT. Experimental results from Figures 12 and 13 in the green row. White rows give the results for a 33-atom active-site model. Yellow rows correlate more (217 atoms) and all (QM/MM) of the protein.

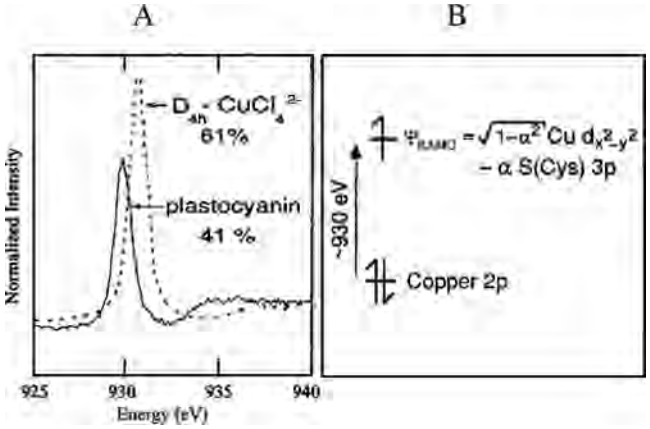

Figure 12. Cu L-edge XAS as a probe of the ligand-to-metal covalency. (A) XAS Cu L_3-edge spectra for D_{4h} $[CuCl_4]^{2-}$ and plastocyanin. Values listed are the amounts of Cu 3d character in the RAMO. (B) Energy-level diagram depicting the Cu 2p to RAMO transition.

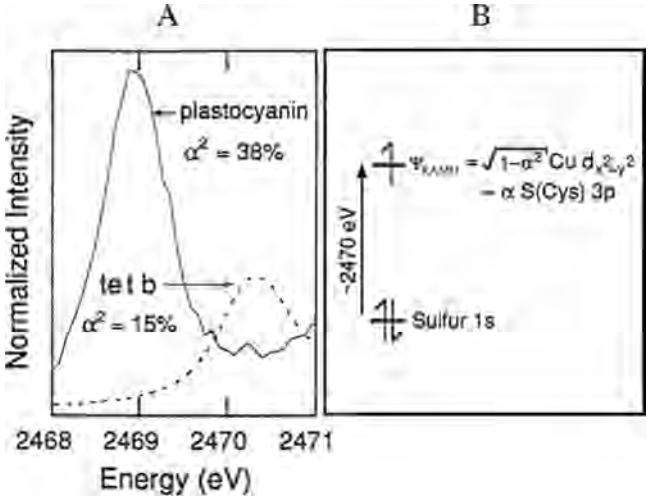

Figure 13. S K-edge XAS as a probe of ligand-to-metal covalency. (A) Orientation-averaged XAS S K-edge spectra for *tet* b [a model complex with a normal Cu^{II}−S(thiolate) bond] and plastocyanin. α^2 is the amount of S p character in the RAMO. (B) Energy-level diagram depicting the S 1s to RAMO transition.

Alternatively, with increased computer power, it is now possible to include a large portion of the protein in the quantum mechanics (QM) calculations (Figure 11 left) or the entire protein using QM/MM methods (yellow rows in the table in Figure 11). These can give very good agreement with experiment because there are two contributions of the protein that reduce the covalency of the thiolate−Cu bond.[27] The first is the hydrogen-bond interaction of the thiolate with a nearby amide, which we have studied in detail for the iron−sulfur proteins.[28] There is also a contribution from the protein dipoles to the decreased covalency of the thiolate−Cu bond.

New Spectroscopic Methods. In this presentation, we focus on spectroscopic methods that experimentally quantify the ground state of blue copper: the amount of metal d character, the S p character, and the π interaction of the $d_{x^2-y^2}$ orbital with the thiolate in Figures 10 and 11.

The amount of Cu d character in the ground state was determined by Cu L-edge spectroscopy.[29] From Figure 12B, at 930 eV one excites electrons from the filled Cu 2p core orbital into the half-occupied RAMO. Because 2p is localized on the copper center and p → d is electric-dipole-allowed, the intensity of this L-edge transition quantifies the amount of Cu $d_{x^2-y^2}$ character in the ground state. From Figure 12A, the blue Cu L-edge is less intense than that of square-planar $CuCl_4^{2-}$, indicating that the blue copper site has less metal d character and is thus more covalent. From studies of square-planar $CuCl_4^{2-}$ using many spectroscopic and computational methods, we know that it has 61% Cu character in its ground state.[30] The intensity in Figure 12A then quantifies the blue copper site as having 41% $d_{x^2-y^2}$ character, very covalent but not as covalent as that in a B3lyp calculation of the copper site in the white rows of the table in Figure 11.

The covalency of the thiolate S−Cu bond can be quantified by S K-edge spectroscopy.[18] We have been developing ligand K-edge spectroscopy as a direct probe of covelancy[28] because this probes all half-occupied and unoccupied valence orbitals and does not require the site to be EPR-active. From Figure 13B, at 2470 eV an electron is excited from the filled S 1s core orbital into the RAMO. Because the 1s orbital is localized on the sulfur and s → p is electric-dipole-allowed, the S K-edge intensity quantifies the amount of S 3p character in the RAMO. From Figure 13A, the blue copper site in plastocyanin has much higher S K-edge intensity and is therefore more covalent[18] than tet b, a model complex[31] with a fairly normal Cu−S bond (Cu−S bond length of 2.36 Å) having 15% S character in its ground state. From the intensity ratio in Figure 13A, the ground state of the blue copper site has 38% Cys S 3p character.

The final feature of the ground-state wave function of the blue copper center is its orientation in the *xy* plane. This derived from low-temperature MCD spectroscopy and relates to the assignment of the unique absorption feature of the blue copper site.[32] From Figure 14Ai and ii, upon going to low temperature and combining absorption/CD and MCD, with each method governed by a different selection rule, there are eight transitions required to fit the electronic spectrum of blue copper in the near-IR−UV−vis region. Band 4 in Figure 14Aii is the characteristic intense, low-energy absorption feature of blue copper at ~16 000 cm^{-1}, and there is an additional weak, lower-energy feature in the low-temperature absorption spectrum, band 6. Polarized single-crystal absorption data in Figure 14Aiii showed that both bands have the same polarization ratio and from correlation to the crystallography are associated with the Cys S−Cu bond.[17] At this point, one might assign the spectrum in parallel to normal copper in Figure 4, a low-energy, weak π and a higher-energy, intense σ charge-transfer transition (Figure 14C

(20) Penfield, K. W.; Gewirth, A. A.; Solomon, E. I. *J. Am. Chem. Soc.* **1985**, *107*, 4519.
(21) Slater, J. C.; Johnson, K. H. *Phys. Rev. B* **1972**, *5*, 844.
(22) Norman, J. G., Jr. *Mol. Phys.* **1976**, *31*, 1191.
(23) Davidson, E. R.*Chem. Rev.* **2000**, **100** (thematic issue).
(24) Ziegler, T.; Autschbach, J. *Chem. Rev.* **2005**, *105*, 2695.
(25) Pierloot, K.; Dekerpel, J. O. A.; Ryde, U.; Olsson, M. H. M.; Roos, B. O. *J. Am. Chem. Soc.* **1998**, *120*, 13156.
(26) Szilagyi, R. K.; Solomon, E. I. *Curr. Opin. Chem. Biol.* **2002**, *6*, 250.
(27) Gorelsky, S. I.; Solomon, E. I., to be published.
(28) Solomon, E. I.; Hedman, B.; Hodgson, K. O.; Dey, A.; Szilagyi, R. K. *Coord. Chem. Rev* **2005**, *249*, 97.
(29) George, S. J.; Lowery, M. D.; Solomon, E. I.; Cramer, S. P. *J. Am. Chem. Soc.* **1993**, *115*, 2968.
(30) Didziulis, S. V.; Cohen, S. L.; Gewirth, A. A.; Solomon, E. I. *J. Am. Chem. Soc.* **1988**, *110*, 250.
(31) Hughley, J. L.; Fawcett, T. G.; Rudich, S. M.; Lalancette, R. A.; Potenza, J. A.; Schugar, H. J. *J. Am. Chem. Soc.* **1979**, *101*, 2617.
(32) Gewirth, A. A.; Solomon, E. I. *J. Am. Chem. Soc.* **1988**, *110*, 3811.

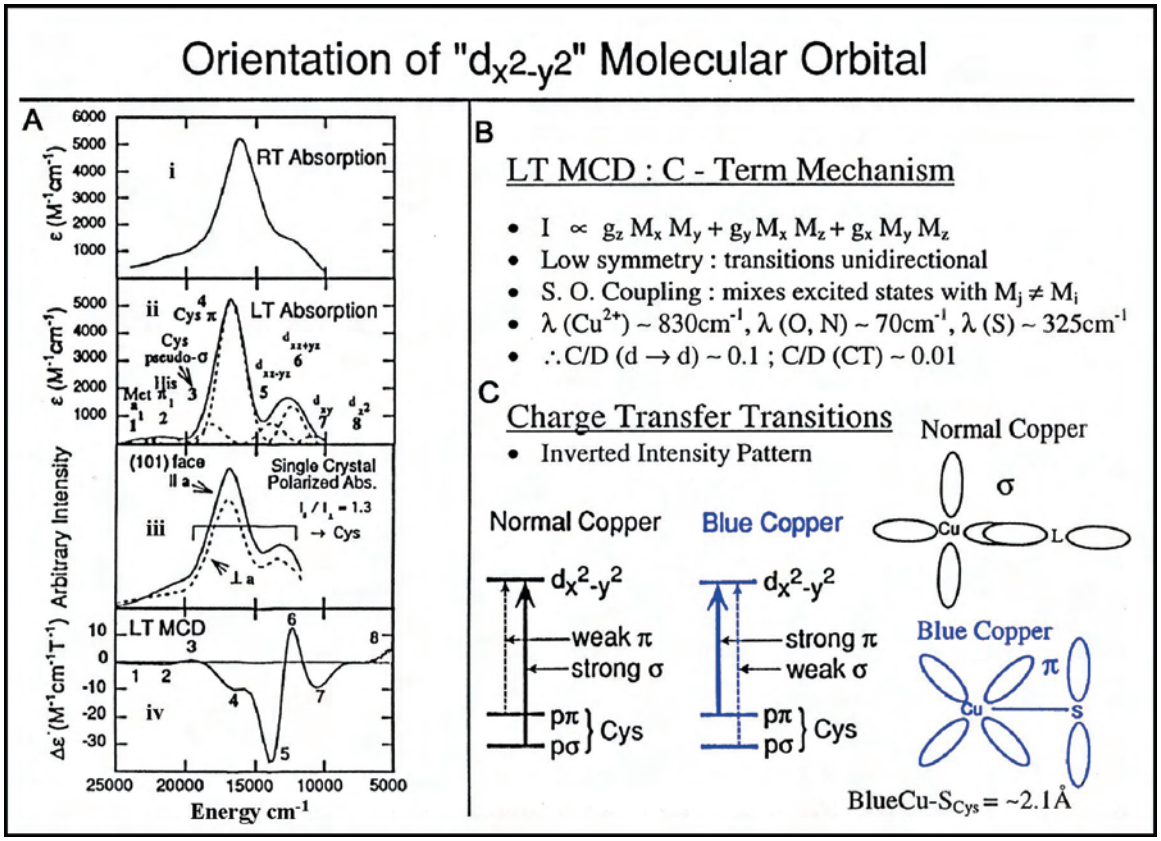

Figure 14. Blue copper excited-state spectral features: (Ai) room-temperature absorption, (Aii) low-temperature absorption, (Aiii) single-crystal polarized absorption, and (Aiv) low-temperature MCD spectrum of plastocyanin. (B) C-term mechanism of low-temperature MCD intensity. (C) Charge-transfer pattern of normal copper (lobe of the $d_{x^2-y^2}$ orbital along the L−Cu bond) and blue copper (lobes bisected by the S−Cu bond).

black). However, this is, in fact, not the case, as revealed by low-temperature MCD spectroscopy. Figure 14Aiv shows that bands 5−8, which are weak in absorption, are the most intense features in the low-temperature MCD spectrum.

Low-temperature MCD intensity involves a *C*-term mechanism,[33] which, as shown in Figure 14B, requires two perpendicular transition moments (M_iM_j, $i \neq j$). In a low-symmetry protein site, all states are nondegenerate and all electronic transitions will thus be unidirectional. Therefore, to get the MCD intensity, one has to spin−orbit couple two excited states with transition moments in different directions. Because the spin−orbit coupling parameter of the metal center is much larger than those of the ligands, the MCD intensity will reflect metal character in the excited states. Therefore, ligand-field transitions will be weak in absorption but intense in MCD.[32] Bands 5−8 in Figure 14A can then be assigned as ligand-field transitions, with the specific assignments based on MCD signs given at the top of Figure 14Aii. Importantly, band 4, which is the most intense feature in the absorption spectrum, is very weak in MCD and must thus be assigned as a low-energy Cys π charge-transfer transition, while a higher-energy, weak band is the Cys σ charge transfer. Therefore, the blue copper site has an inverted charge-transfer pattern (Figure 14C): low-energy, intense π/high-energy, weak σ. Because the charge-transfer intensity reflects orbital overlap, this requires that the $d_{x^2-y^2}$ orbital be rotated such that its lobes bisect the Cu−S Cys bond rather than be oriented along the bond as in normal copper complexes.[32] This occurs because of the strong π-antibonding interaction of Cys S with the metal d orbital due to its short 2.1-Å bond length.

Electronic Structure Contributions to ET. Having developed a detailed description of the electronic structure of blue copper, we can now correlate this with its efficiency in biological ET. As discussed above, two factors are required: a large $\mathbf{H}_{DA}$ and a small λ.

H_{DA}: Superexchange Pathways. In Figure 15A, the RAMO developed above has been superimposed over a portion of the structure of the blue copper site in the multicopper oxidases. These enzymes are particularly interesting in that the ET pathway is reasonably well defined. The electron enters at the blue copper site. Its thiolate ligand is flanked on either side in the sequence by His's, which are ligands to a trinuclear copper cluster site.[34] Electrons are transferred from the blue copper to the trinuclear copper cluster, where dioxygen is reduced to water.[35] From Figure 15A, the high anisotropic covalency of the Cu−S thiolate bond clearly activates the Cys−His pathway for rapid directional ET[36] to the trinuclear copper site.

We have recently focused on determining the superexchange pathways through the protein for this ET.[27] Figure 15B gives a description of the molecular orbital delocalized

(33) Piepho, S. B.; Schatz, P. N. *Group Theory in Spectroscopy with Applications to Magnetic Circular Dichroism*; John Wiley & Sons: New York, 1983.

(34) Allendorf, M. D.; Spira, D. J.; Solomon, E. I. *Proc. Natl. Acad. Sci.* **1985**, *82*, 3063.

(35) Solomon, E. I.; Sundaram, U. M.; Machonkin, T. E. *Chem. Rev.* **1996**, *96*, 2563.

(36) Lowery, M. D.; Guckert, J. A.; Gebhard, M. S.; Solomon, E. I. *J. Am. Chem. Soc.* **1993**, *115*, 3012.

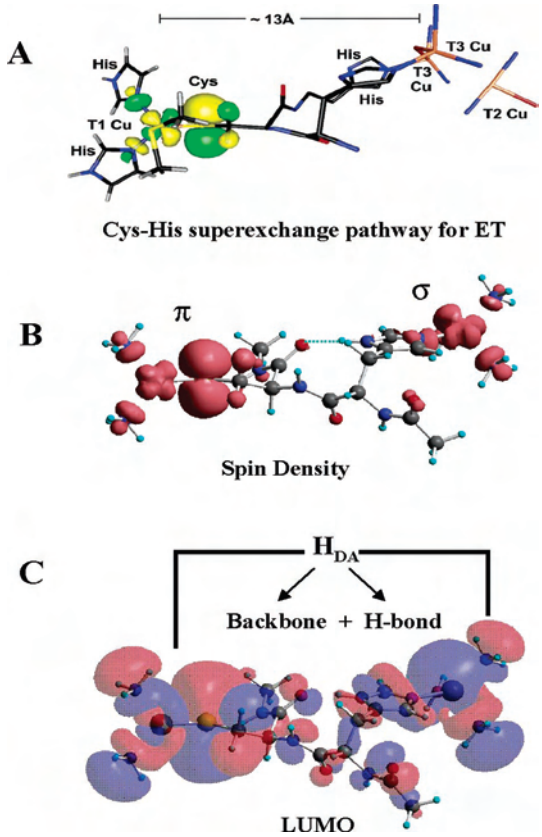

Figure 15. Superexchange pathway of the blue copper site: (A) RAMO superimposed on part of the crystal structure of a multicoppper oxidase; (B) π-to-σ hole delocalization between blue copper and a remote copper center; (C) π-to-σ superexchange pathways through a Cys−His molecular orbital.

between the Cu−S π bond on blue copper and the N−Cu σ interaction on the acceptor copper. From the contour in Figure 15C, there are two contributions to this superexchange pathway. The thiolate π bond is oriented such that it delocalizes into the protein backbone, which is then σ bonded to the His ligand at the remote copper. There is also a π-to-σ H-bond overlap, which is small but the pathway is shorter. These contributions to $\mathbf{H}_{DA}$ can be comparable (depending on the H-bond distance) and constructive in that they both increase the highest occupied molecular orbital/lowest unoccupied molecular orbital splitting and therefore $\mathbf{H}_{DA}$.

λ: Change in Geometric and Electronic Structures with Oxidation. To understand the change in the geometric structure with oxidation of the blue copper site, we need to consider its change in electronic structure. Therefore, attention is now focused on the reduced blue copper site. This has a d^{10} configuration and cannot be studied by the above open-shell spectroscopic methods. Thus, variable-energy photoelectron spectroscopy was utilized to probe its electronic structure and how this changes with ionization.[37] Because in this method electrons are detected with escape depths on the order of 10 Å, these studies needed to be performed on model complexes. Further, because an important issue in blue copper has been the role of the protein in determining the geometric structure, these studies focused on unconstrained models. Our strategy was thus to chemisorb the blue-copper-relevant imidazole, dimethyl sulfide, and methylthiol ligands to coordinatively unsaturated Cu^{I} sites on oxide and chloride single-crystal surfaces in ultrahigh-vacuum. Figure 16A shows methylthiolate chemisorbed on $Cu_2O(111)$ as an example, where the oxide was used to drive the deprotonation reaction. The dashed spectrum is for clean

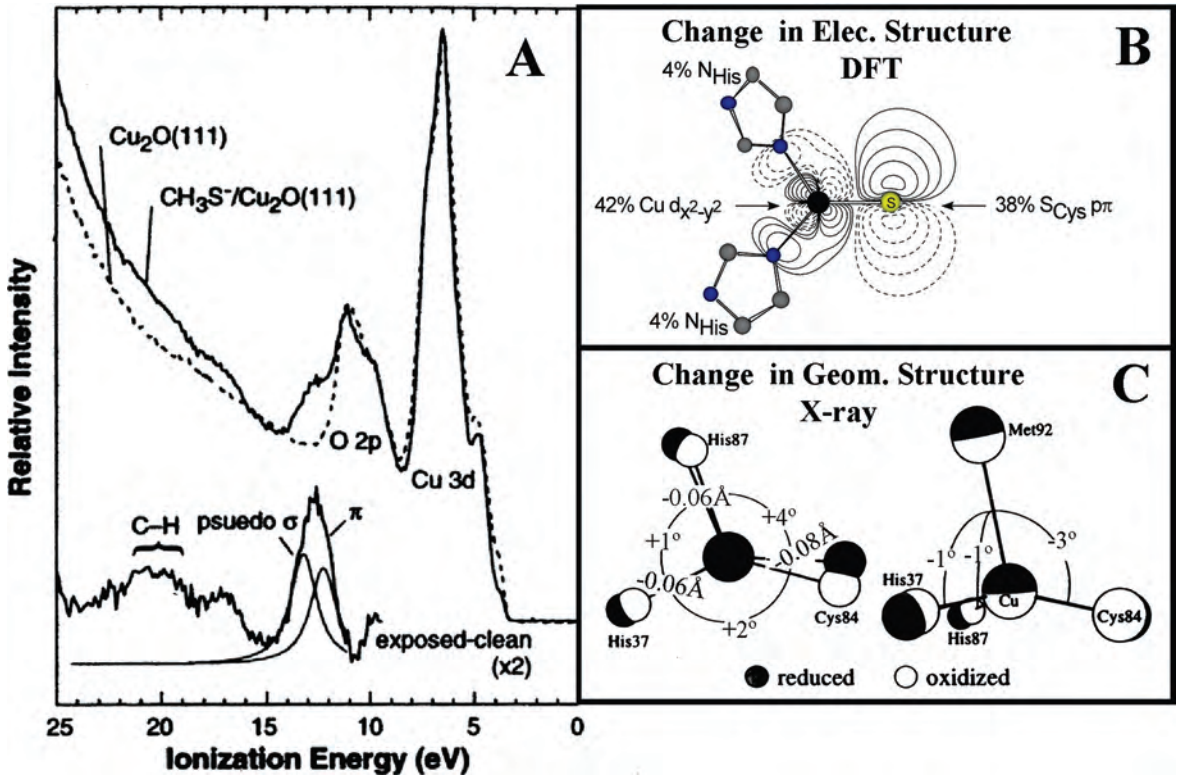

Figure 16. $Cu^{I}-SCH_3$ bonding: (A) valence-band spectrum of $Cu_2O(111)$ (dotted line), $Cu_2O(111)$ exposed to methane−thiol (solid line), and their difference spectrum (bottom) with Gaussian/Lorentzian resolution of the low-energy region; (B) RAMO giving changes in the electronic structure of blue copper upon oxidation; (C) average structural changes upon oxidation of a blue copper site (amino acid numbering from plastocyanin). Bond lengths are based on EXAFS results. Angular changes are based on crystallographic results.

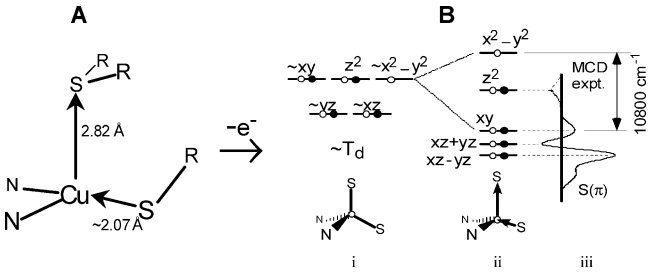

Figure 17. Protein constraint: reduced blue copper site. (A) Effects of the protein on the ligand donor interactions in blue copper sites. Arrows show decreased electron donation from the axial S(Met), which results in increased electron donation from the S(Cys). (B) Schematic of the blue copper ligand-field effect on the oxidized site. The Jahn−Teller distorting force is eliminated, which minimizes the reorganization energy of the site. (Bi) Energy-level diagram of an idealized T_d structure that is subject to a Jahn−Teller distortion upon oxidation, while the (Bii) C_s structure of the blue copper site is not. (Biii) MCD spectrum of plastocyanin, showing that the $d_{x^2-y^2}$ and d_{xy} orbitals are split by over 10 000 cm^{-1}, eliminating the Jahn−Teller distorting force of the oxidized site.

Cu_2O. The solid spectrum is for methylthiolate chemisorbed to Cu_2O, and the difference at the bottom reflects the valence orbitals of thiolate split in energy due to bonding to Cu^I. These were studied as a function of photon energy using synchrotron radiation. The intensity changes allowed the assignment of specific peaks and a quantitation of the wave functions from which the electrons are ionized.[38] The data on the surface complexes were used to calibrate DFT calculations, and calculations supported by the data were used to construct the electronic structure description of the reduced blue copper site and to determine how this changes upon oxidation.[37]

From Figure 16B, the dominant change upon oxidation is simply the hole produced in the RAMO. This eliminates antibonding interactions of the copper with the thiolate S and two His N ligands. Thus, upon oxidation there are distorting forces to contract these bonds. From crystallography[39,40] combined with EXAFS[19,41] on going from the reduced (solid atoms in Figure 16C) to the oxidized site (open atoms), the Cys S−Cu and His N−Cu bonds contract. Importantly, there is no distorting force along a bending mode and few angular changes are observed in the crystal structures.

If the protein were, in fact, opposing a Jahn−Teller tetragonal distortion of the oxidized site, there would be a distorting force along a bending mode. The protein constraint that appears to be present at the blue copper site is the long thioether S−Cu bond in the reduced structure (~2.9 Å; an unconstrained Cu−S Met bond would be ~2.4 Å).[37] This long bond reduces the donor interaction of the thioether with the copper, which is compensated for by the thiolate, leading to the short 2.1-Å Cu−S Cys bond (Figure 17A). This long thioether/short thiolate combined distortion has an important effect on the oxidized blue copper site. Starting from the tetrahedral limit (Figure 17 Bi), there would be one hole in the t_2 set of d orbitals, which is degenerate and unstable to a Jahn−Teller tetragonal distortion. However, the long thioether/short thiolate ligand field leads to a large d orbital

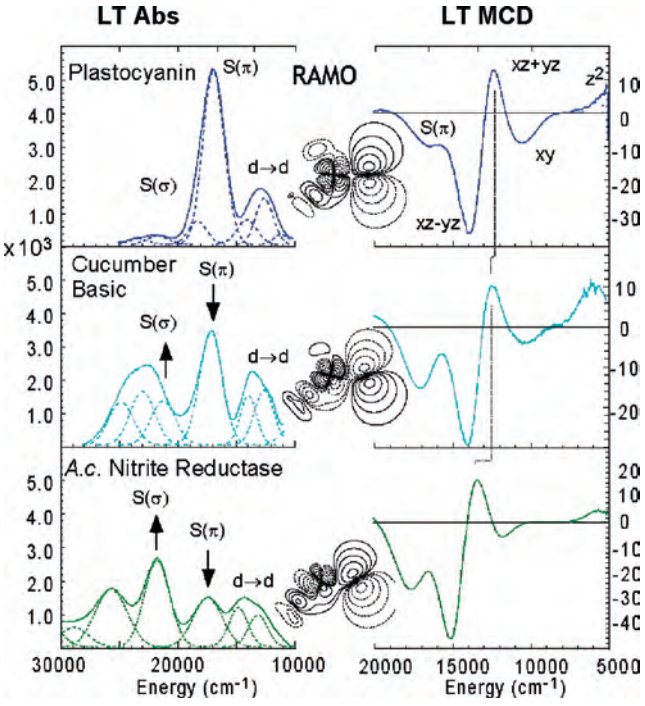

Figure 18. Coupled distortion coordination in a series of perturbed blue copper proteins. Low-temperature absorption showing redistribution of the spectral intensity from Cys π-to-σ charge-transfer bands. Redox-active orbitals calculated with SCF-Xα-SW showing rotation from a π-type interaction in plastocyanin (left top) to a σ ($+\pi$) mixture in nitrite reductase (left bottom). MCD spectra showing a shift of the ligand-field transitions to higher energy for nitrite reductase relative to plastocyanin, indicating a tetragonal distortion.

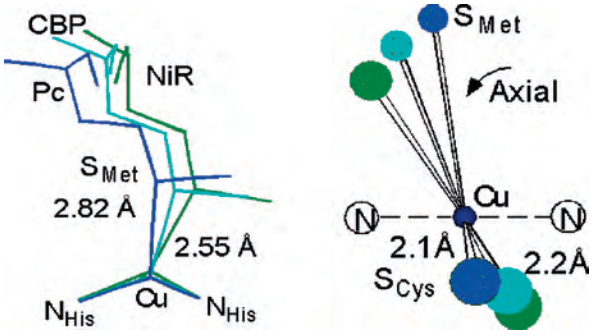

Figure 19. Continuum of coupled tetragonal distortions in a series of perturbed blue copper proteins. Crystal structures[39,43,44] show contraction of the Cu−S(Met) bond associated with elongation of the Cu−S(Cys) bond and tetragonal ϵ_u-like mode Jahn−Teller distortion.

splitting in the oxidized state (Figure 17 Bii). In particular from Figure 17Biii, the $d_{x^2-y^2}$ splitting is ~10 000 cm^{-1} from MCD (Figure 14Aii). Electron−nuclear coupling between these levels, when close to degenerate, would lead to a tetragonal Jahn−Teller distorting force. Thus, this is not present; there is a fairly limited geometry change and small reorganization energy upon oxidation. Clearly, this active site is well-tuned for rapid outer-sphere ET, and we now consider the role of the protein in determining the geometric and electronic structures of the blue copper site.

Role of the Protein in Active-Site Geometric and Electronic Structures. Figure 17 leads to a coupled distortion model where the long thioether−Cu bond results in a short thiolate−Cu bond, and together these eliminate the Jahn−Teller tetragonal distortion of the oxidized site. This coupled distortion model explains the spectral features of a

(37) Guckert, J. A.; Lowery, M. D.; Solomon, E. I. *J. Am. Chem. Soc.* **1995**, *117*, 2817.
(38) Solomon, E. I.; Basumallick, L.; Chen, P.; Kennepohl, P. *Coord. Chem. Rev.* **2005**, *249*, 229.
(39) Guss, J. M.; Bartunik, H. D.; Freeman, H. C. *Acta Crystallogr., Sect. B* **1992**, *48*, 790.
(40) Guss, J. M.; Harrowell, P. R.; Murata, M.; Norris, V. A.; Freeman, H. C. *J. Mol. Biol.* **1986**, *192*, 361.
(41) Ellis, P. J., University of Sydney, Sydney, Australia, 1995.

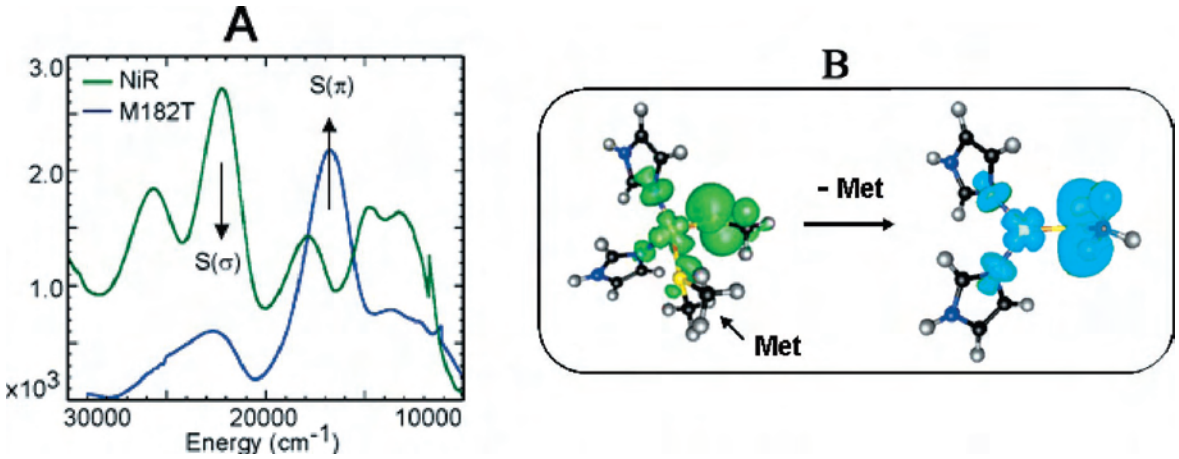

Figure 20. Comparison of the spectral features of Met182Thr mutant and wild-type nitrite reductase: (A) low-temperature absorption spectra; (B) geometry-optimized DFT with (green) and without (blue) the Met ligand.

series of blue-copper-related proteins that all have the same Cys, two His, and Met ligand set but vary from blue in plastocyanin to green in some nitrite reductases.[42] From Figure 18 left, it can be seen that over this series the π charge transfer goes down in intensity and the σ charge transfer (hence, σ overlap with the copper) becomes dominant in the green site. The MCD data for the ligand-field transitions in Figure 18 right show that, over this series, the d → d transitions shift up in energy, indicating a tetragonal distortion of the copper site. From superposition of the crystal structures of plastocyanin,[39] cucumber basic blue,[43] and nitrite reductase[44] in Figure 19, it is observed that, in going from the blue to the green copper, the Met S−Cu bond length decreases, the Cu−S Cys bond length increases, and there is a tetragonal rotation of the S−Cu−S plane into the N−Cu−N plane, indicating a Jahn−Teller distortion in the green site.

The fact that these proteins all have the same ligand set yet exhibit a large change in geometric and electronic structures clearly demonstrates that the protein can tune the structure of the metalloprotein active site. The role of the Met ligand in this coupled distortion coordinate has been evaluated by mutating off the relatively strong Met ligand in the green site in nitrite reductase.[45] As shown in Figure 20A, the site goes from having its σ charge transfer being dominant in the green site to the π charge transfer being the dominant feature of the resultant blue site. This behavior was reproduced in DFT calculations. From Figure 20B, geometry optimization of the blue copper ligand set with no constraint leads to a fairly short thioether S−Cu bond and a green site with the thiolate having a σ bond to the copper. If Met is removed and the site is reoptimized, the $d_{x^2-y^2}$ orbital rotates and the thiolate now π interacts with the copper, correlating with the intense π-charge-transfer transition of the blue site.

Finally, these studies have recently been extended to the red copper site in nitrosocyanin and related proteins (Figure 21).[46] For this class of sites, the relatively weak Met axial ligand is replaced by a strong His ligand and the strong His equatorial ligand is replaced with a weak Glu carboxylate ligand.[47] This effectively rotates the equatorial plane of the

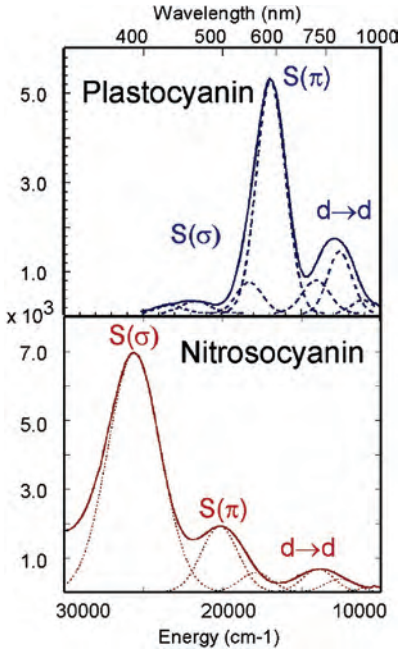

Figure 21. Absorption spectrum of red copper (bottom) compared to that of the blue copper site (top).

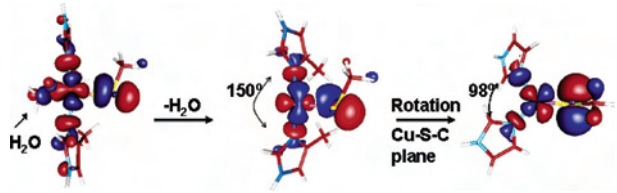

Figure 22. Contour plots for ground-state wave functions of (A) five-coordinate red copper and (B) four-coordinate (water ligand eliminated) red copper optimized with the C−S−Cu plane oriented in the molecular plane and (C) with the C−S−Cu plane rotated normal to the equatorial plane and reoptimized. The axial ligands are not shown to visualize the bonding differences in the red and blue copper sites.

(42) LaCroix, L. B.; Randall, D. W.; Nersissian, A. M.; Hoitink, C. W. G.; Canters, G. W.; Valentine, J. S.; Solomon, E. I. *J. Am. Chem. Soc.* **1998**, *120*, 9621.
(43) Guss, J. M.; Merritt, E. A.; Phizackerley, R. P.; Freeman, H. C. *J. Mol. Biol.* **1996**, *262*, 686.
(44) Adman, E. T.; Godden, J. W.; Turley, S. *J. Biol. Chem.* **1995**, *270*, 27458.
(45) Basumallick, L.; Szilagyi, R. K.; Zhao, Y.; Shaphigh, J. P.; Sholes, L. P.; Solomon, E. I. *J. Am. Chem. Soc.* **2003**, *125*, 14784.
(46) Basumallick, L.; Sarangi, R.; George, S. D.; Elmore, B.; Hooper, A. B.; Hedman, B.; Hodgson, K. O.; Solomon, E. I. *J. Am. Chem. Soc.* **2005**, *127*, 3531.
(47) Lieberman, R. L.; Arciero, D. M.; Hooper, A. B.; Rosenzweig, A. C. *Biochemistry* **2001**, *40*, 5674.

copper into the Cu−S−C plane, and the copper binds an additional equatorial water ligand. For the red copper site (Figure 22 left), the thiolate is now σ-bonding to the copper (thus, the σ-charge-transfer transition is dominant in Figure 21 bottom) and the additional water donor ligand raises the energy of the d manifold, which shifts the σ charge transfer up in energy relative to this transition in the green copper site.

Calculations supported by the data were further used to obtain insight into the issue of why only this class of blue-copper-related sites is able to bind an exogenous water ligand. From Figure 22 center, removal of the water ligand and reoptimization leads to a site that still has the thiolate σ bond to the copper and the open equatorial coordination position for exogenous ligand bonding. However, rotation of the thiolate C−S−Cu plane so that it is now perpendicular to the equatorial copper plane (Figure 22 right) results in a π interaction of the thiolate with the copper, which rotates the half-occupied $d_{x^2-y^2}$ orbital. The His ligands move in to maximize their overlap with this orbital, and this eliminates the open coordination position. Thus, by variation of two ligands, nature has converted the blue copper site, which is efficient in outer-sphere ET with a low λ and large $\mathbf{H}_{DA}$, to a red copper site, which has a large λ and small $\mathbf{H}_{DA}$ but is now efficient in inner-sphere ET.[48]

(48) Basumallick, L.; Xie, X.; Solomon, E. I.; Hooper, A. B., to be published.

Summary. This presentation has emphasized the fact that different spectroscopic methods provide complimentary insight into an active site, and the appropriate combination of methods will provide detailed experimental insight into the electronic structure. It is of critical importance to correlate spectroscopy with the results of electronic structure calculations, and together these give maximum insight into reactivity. Finally, the unique spectroscopic features exhibited by many classes of active sites in bioinorganic chemistry (i.e., intense absorption bands, unusual ground-state parameters, etc.) reflect novel geometric and electronic structures that can make major contributions to function.

Acknowledgment. For this general presentation, I want to recognize my past and present graduate students and postdocs who have had the intelligence, drive, and creativity to make this science happen. I also want to thank a wonderful group of collaborators who have made amazing biological and inorganic molecules and unique instrumentation available for our studies. Finally, I want to thank NIH (Grants DK 31450 and GM 40392) and NSF (Grants CHE 0446304 and MCB 0342807) for funding basic research that has had an important impact in biotech, environmental, catalytic, and health-related applications. The assistance of Xiangjin Winson Xie in the preparation of this manuscript is acknowledged.

IC060450D